

Discrimination of Mechanical Response to ARFI Excitation in a Raised Atherosclerotic Plaque

Joshua H. Levy¹, Russell Behler², Mansoor A. Haider³, J. S. Marron⁴, and
Caterina M. Gallippi²

¹ Department of Computer Science,
University of North Carolina at Chapel Hill levy@cs.unc.edu,

² Joint Department of Biomedical Engineering,
University of North Carolina at Chapel Hill and North Carolina State University,

³ Department of Mathematics, North Carolina State University,

⁴ Department of Statistics and Operations Research,
University of North Carolina at Chapel Hill

Abstract. Acoustic Radiation Force Impulse (ARFI) is a noninvasive ultrasound modality that differentiates tissue structure via viscoelastic property. We are interested in using ARFI to discriminate between non-atherosclerotic arterial walls and atherosclerotic plaque. Both of these tissue types can be modeled as Kelvin materials each characterized by its own elasticity and viscosity. These properties define the displacement and recovery of tissue in response to ARFI. In this paper we present algorithms for clustering ARFI-induced displacement curves and we use the Kelvin model as a filter for outlier rejection. We validated these algorithms against a synthetic data set and then obtained preliminary results for an ARFI image of a raised focal atherosclerotic plaque in a porcine iliac artery.

1 Introduction

Cardiovascular disease (CVD) is the leading cause of death in North America [1]. Because atherosclerotic plaques exhibit different material (i.e. mechanical) properties than non-atherosclerotic arterial wall, measurement of tissue mechanical properties is relevant to diagnosis and monitoring CVD status. Conventionally, arterial mechanical properties could not be measured directly, and surrogate metrics such as peripheral pulse pressure and pulse wave velocity have been used to infer systemic arterial mechanical properties [2]. Recently, the direct localized measurement of arterial mechanical properties has been made possible by the following advances in ultrasound technology: intravascular ultrasound (IVUS) elastography, non-invasive vascular elastography (NIVE), and acoustic radiation force impulse (ARFI) ultrasound.

IVUS uses a catheter ultrasound probe to image a cross-section of a blood vessel intravascularly. Using controlled pull-back, multiple correlated IVUS images are acquired during physiological arterial pulsation. The images are then processed as in ultrasound elastography to compute local strain, which is displayed parametrically in the form of an elastogram image. Van der Steen et al [3] have implemented IVUS elastography to produce images of the Young's Modulus of tissue and have applied a shape model to segment the boundary between atherosclerotic plaque and arterial wall in the Young's Modulus elastogram. Although IVUS elastography has been demonstrated for effective differentiation of atherosclerotic from nonatherosclerotic tissue, IVUS requires

a significant amount of time for preparation and for imaging. Because the procedure is invasive, it can produce serious side effects including the dislodgement of a plaque, post-procedural hemorrhaging, and hematoma formation during catheter insertion.

NIVE is a noninvasive technique that has been used to create Von Mises coefficient elastograms of superficial arteries [4]. NIVE uses the Lagrangian speckle model estimator to recover strain tensors from high frequency ultrasound images during the normal pulsation of the artery.

ARFI ultrasound is another noninvasive modality for measuring the mechanical properties of tissue. ARFI ultrasound is performed transcutaneously using a conventional ultrasound system (modified for research purposes) and transducer. In ARFI imaging, momentum is transferred from a short duration acoustic impulse to tissue in a manner that displaces tissue on the order of microns. Following the displacing, or pushing, impulse, multiple conventional A-lines are acquired in ensemble form to track induced axial tissue displacement and subsequent recovery via one-dimensional cross-correlation. ARFI imaging can be implemented two-dimensionally to assess tissue mechanical properties over both space and time [5]. We present here preliminary results towards characterizing atherosclerotic plaques by automatic ARFI image segmentation.

For the purpose of segmenting ARFI-induced tissue displacement curves, we assume that arterial walls and atherosclerotic plaques can be idealized as Kelvin materials. For either tissue type the equation

$$F + \tau_\epsilon \dot{F} = E_R (u + \tau_\sigma \dot{u}) \quad (1)$$

holds [6]. Here F is the applied force, u is the extension of the material, and $\tau_\epsilon, \tau_\sigma$ are the relaxation times for constant-strain and constant-stress respectively for the material. E_R is the relaxed elastic modulus for the material and $\dot{\cdot}$ denotes differentiation with respect to time.

We model the force from ARFI as $F(t) = f_0 (H(t) - H(t - \epsilon))$ where H is the Heaviside function and ϵ is the impulse duration [7]. At time $t > \epsilon$,

$$u(t) = u_0 \exp\left(-\frac{t}{\tau_\sigma}\right) \quad (2)$$

$$u_0 = \frac{f_0}{E_R} \left(\exp\left(\frac{\epsilon}{\tau_\sigma}\right) - 1 \right) \frac{\tau_\sigma - \tau_\epsilon}{\tau_\sigma} \quad (3)$$

We expect that the ARFI-induced displacement curve for a Kelvin material will show peak initial displacement followed by an exponential recovery time. The ARFI response curve for a tissue is influenced by material properties of the tissue. Our method characterizes different Kelvin materials (i.e. plaque and arterial wall) based on their ARFI-induced displacement curves without directly estimating the Young's modulus [8, 2, 3] or the Von Mises coefficient [4] for the different tissue classes.

2 Method

Our problem is then to cluster samples from a two parameter family of exponential decay curves (2). In Sec. 2.1 we discuss algorithms for clustering these curves. In Sec. 2.2 we apply these clustering algorithms to simulated data. In Sec. 2.3 we discuss a preliminary experiment of clustering the ARFI response of a raised focal atherosclerotic plaque in an excised iliac artery.

2.1 Clustering

An ARFI image of size $x \times y \times t$ measures the displacement of $x \cdot y$ tissue samples at t time steps. Let $\mathbf{f}_{i,j}$ denote the t -dimensional vector of displacements at position (i, j, \cdot) in the image. We wish to cluster $\{\mathbf{f}_{i,j} : 1 \leq i \leq x, 1 \leq j \leq y\}$ via the k -means [9] algorithm.

Much of the work performed by the k -means algorithm is distance calculations. The number of multiplications performed in each distance calculation is proportional to the dimensionality of the feature space. Reducing the dimensionality of the feature space is desirable because it allows for faster clustering. This is especially important because k -means tends to find locally optimal clusters. It is common practice to seek the best locally optimal clustering from multiple repetitions of the algorithm run from different random starting points.

For a displacement curve of the form (2), $\mathbf{f}_{i,j}$ contains redundant information. We can reduce the dimensionality of this space by estimating the parameters of the exponential curve for each displacement vector. A nonlinear least squares optimization estimates the parameters

$$\mathbf{g}_{i,j} = \{\hat{c}, \hat{r}\} = \arg \min_{c,r} \|c \exp(-r\mathbf{T}) - \mathbf{f}_{i,j}\|^2 \quad (4)$$

where \mathbf{T} is a vector of time steps consistent with the sampling in \mathbf{f} . This representation has the advantage of being compact, but the interpretation of clustering can be uncertain because the parameters c and r are not commensurate.

Principal components analysis (PCA) is another mechanism for reducing the dimensionality of the displacement vectors. PCA treats each $\mathbf{f}_{i,j}$ as a single point in a linear t -dimensional space. Let μ denote the mean and Σ the covariance of these points. Let the eigenvalues and eigenvectors of Σ be denoted by $\{\lambda_i : 1 \leq i \leq t\}$ and $\{\mathbf{v}_i : 1 \leq i \leq t\}$ respectively. Assuming that the eigenvectors are sorted by descending eigenvalue, $j \leq k \leftrightarrow \lambda_j \geq \lambda_k$, the dimensionality of the feature space is reduced to $t' \ll t$ by

$$\mathbf{h}_{i,j}^k = \frac{(\mathbf{f}_{i,j} \cdot \mathbf{v}_k)}{\sqrt{\lambda_k}} : 1 \leq k \leq t' \quad (5)$$

The new dimensionality t' is typically chosen to explain a fixed percentage of variance. We will see in Sec. 2.2 that for many of our simulated cases we can explain $> 95\%$ of the variance in the high dimensional space with only a few principal components.

2.2 Simulated Data

We produced simulated data to test these clustering algorithms. We began by producing curves of the form $c \exp(-rt)$ for a variety of parameters c, r . A vector $\mathbf{f}_{i,j}$ is produced by sampling the curve at 60 uniformly spaced time steps and then adding white Gaussian noise to the sampled curves. Figure 1 gives examples of the data with S/N ratios of 32dB, 24dB, and 12dB.

The vectors $\mathbf{f}_{i,j}$ lie in a 60-dimensional space, but from the formulation we expect that the data will lie in a two-dimensional subspace. Two different 2D approximations of the data are calculated: $\mathbf{g}_{i,j}$, by recovering the parameters for each exponential curve, and $\mathbf{h}_{i,j}$ by performing PCA. The result of projecting the curves into the lower dimensional spaces can be seen in Fig. 2.

Note that for the range of c, r used in this experiment that the PCA-based dimensionality reduction appears to be more robust to noise than the parameter

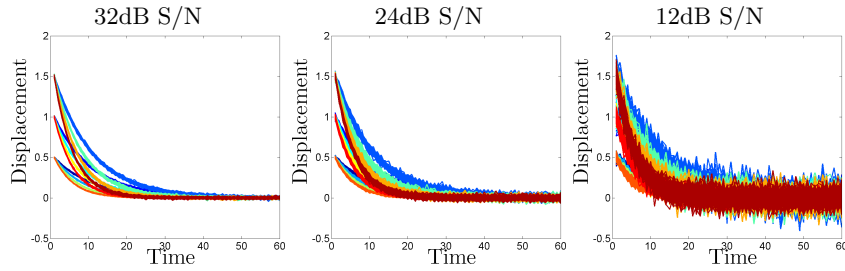


Fig. 1. Simulated curves $f_{i,j}$ with additive white Gaussian noise.

recovery method. Even at the 24dB S/N ratio, 12 distinct clusters, corresponding to the 12 combinations of the two control parameters, are visible and can be easily separated in the PCA image. In the scatter plot of the recovered exponential parameters from the 24dB data there is some overlap between clusters where a curve might be misidentified as having lower c, r parameters than were present in the raw curves before noise was added.

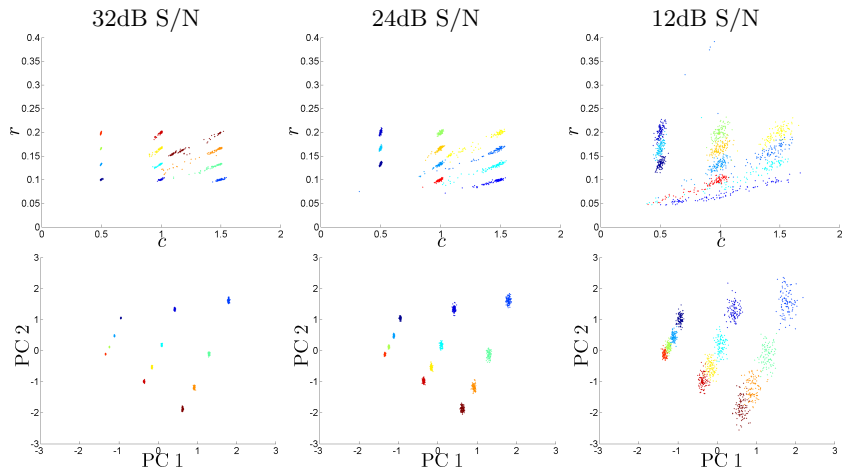


Fig. 2. Dimensionality reduction on the data from Fig. 1. (top) Recovered exponential parameters: (c, r) . (bottom) Projection onto two principal components. Each of the dimensionality reduction schemes transforms all curves with the same parameters to a single point.

Each of our proposed methods of dimensionality reduction has a natural measure of its effectiveness. The percent of residual variation,

$$\rho_e = \frac{\|\hat{c} \exp(-\hat{r}\mathbf{T}) - \mathbf{f}_{i,j}\|^2}{\|\mathbf{f}_{i,j}\|^2} \quad (6)$$

gives an indication of how well an individual curve $f_{i,j}$ can be modeled by an exponential. This ratio is bounded by $0 \leq \rho_e \leq 1$ with a lower value indicating a better fit of the exponential curve to the sampled data. The distribution of ρ_e for our simulated data is presented in Fig. 3 (a). The percentage of variance

explained,

$$\rho_p(t') = \frac{\sum_{i=1}^{t'} \lambda_i}{\sum_{j=1}^t \lambda_j} \quad (7)$$

measures how well the t' -dimensional PCA approximates the original set of curves. This ratio is bounded by $0 \leq \rho_p(t') \leq 1$ with a greater value indicating that the t' -dimensional approximation is better able to recover the original data. Because the noiseless data came from a two-dimensional space we hope to see $\rho_p(t') \approx 1$ when $t' \geq 2$, even with small amounts of noise present. Figure 3 (b) shows ρ_p for the simulated dataset. Note that two principal components are sufficient to approximate the noiseless data and the curves with a 32dB or a 24dB S/N ratio, but there is significant residual variance when two principal components are used to approximate the 12dB S/N ratio data. This is caused, in part, by the fact that ρ_e is quite large for a significant fraction of the 12dB data. When we process ARFI data we will reject data with large ρ_e prior to performing PCA.

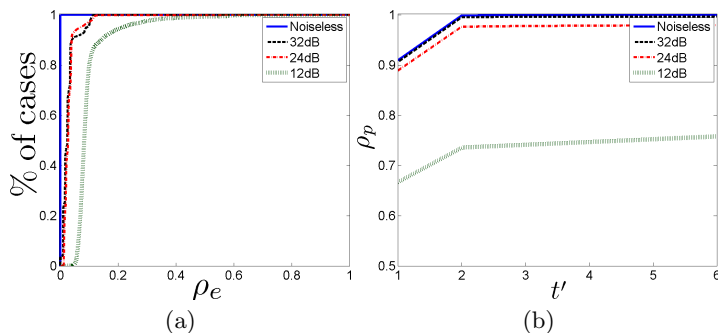


Fig. 3. (a) Cumulative histogram of ρ_e for the data in Fig. 1. (b) ρ_p as a function of t' . As the noise level increases the exponential fits the data less well, ρ_e takes on larger values for a fixed quantile of the curves, and it takes more principal components to explain a fixed amount of variance.

2.3 ARFI Data

Two-dimensional ARFI ultrasound was performed on an excised iliac artery of a familial hypercholesterolemic swine [10]. The imaging field of view included a focal atherosclerotic plaque. Axial tissue motion in response to ARFI excitation was measured with one-dimensional cross-correlation to generate profiles of ARFI-induced tissue displacement over time (a 5 ms observation period, 60 samples). For complete details on the image acquisition protocol we refer the reader to [11].

A B-mode ultrasound image of the same field of view was processed to automatically produce a mask for rejecting signal from fluid in the vessel lumen. In the specific image region of interest (ROI) we studied, this reduced the size of the data from $\sim 100,000$ displacement curves down to 7,500. Figure 4 (a) shows the B-mode image and highlights this ROI.

The optimization (4) is used to estimate the exponentials fit to the ARFI displacement curves. If the Kelvin model applies to both the arterial wall and

the atherosclerotic plaque, the percentage of residual variation (6) should be low for the ARFI displacement curves for these tissues. The image also includes other tissues for which this model need not apply. We do not expect that (2) will approximate well the ARFI displacement curve for such tissue. Because we are not attempting to characterize these other tissues, we discard the curves for which ρ_e is above a threshold level. Discarding data with $\rho_e > 0.15$ left us with a final set of $\sim 6,000$ displacement curves. Examples of the curves accepted and rejected by this filter can be seen in Fig. 4 (b). PCA on these curves showed that with three principal components $\rho_p \approx 0.969$.

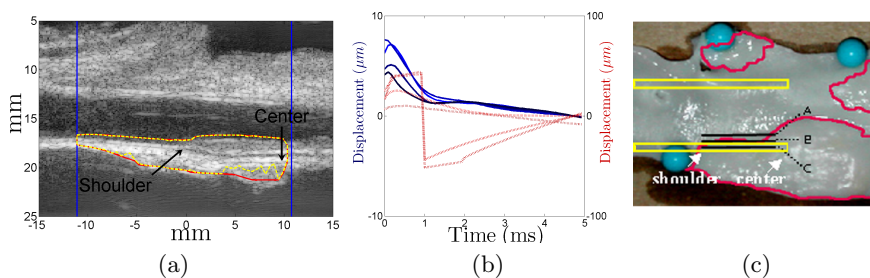


Fig. 4. (a) B-mode ultrasound image of an excised porcine iliac artery. The region for which ARFI data is available is shown in blue. The region identified in an ROI of the B-mode image is indicated in red. The region identified by filtering ARFI data on ρ_e is indicated in yellow. (b) Example ARFI displacement curves with $\rho_e < 0.15$ (solid) and $\rho_e > 0.15$. Some of the curves with high residual variation are due to noise and aliasing. Others may indeed be Kelvin materials, but show a delayed peak in their ARFI response. (c) The open vessel. The yellow boxes indicate the proximal and distal walls visible in (a). Histology of the section labeled *C* is discussed in Fig. 5 (C-D).

3 Results

In our experiments on simulated data we created 500 curves for each of 12 categories corresponding to the parameters of the exponential curve before noise was added. We used the k-means algorithm to recover 12 clusters with hope that each cluster would correspond to a pre-noise category. The false labeling rates listed below were measured as the percentage of curves with different pre-noise parameters from the mode of their cluster.

	32dB	24dB	12 dB
Raw Curves	25.0%	33.3%	34.5%
Exponential Coefficients	10.0%	25.5%	32.0%
PCA Coefficients	8.3%	16.7%	15.5%

The high false labeling rates are not unexpected given that a significant amount of overlap due to noise is visible in Fig. 1. We observed that clustering on PCA coefficients produced the best results for a fixed noise level. It is surprising that the PCA representation was slightly more effective on the 12dB data than on 24dB data. One way that k-means can fail is by producing a cluster with small membership (i.e. only a few outliers) which then forces the creation of a second cluster with large membership and thus many false

labelings. These failures contribute to the apparent mismatch in the results for the clustering of PCA coefficients for the 24dB and 12dB datasets.

We clustered the PCA coefficients of the ARFI displacement curves. A comparison of these clusters with histology performed in the same tissue region shows promising results which we present in Fig. 5. The atherosclerotic plaque is approximately 10mm long. Immunohistochemistry indicated spatially correlated differences in tissue composition of the plaque. Gradation is visible between a high elastin/low collagen content on its left side and a low elastin/high collagen content on its right side. The plaque and its subcomponents are identified as distinct clusters by the k-means algorithm. There is a region within the plaque that appears unclustered (white in the bottom row of Fig. 5). This tissue has suffered severe elastin degradation to the point that its response to ARFI is not consistent with (2) and it is rejected by our filter on ρ_e . The histological results are treated in greater detail in [11].

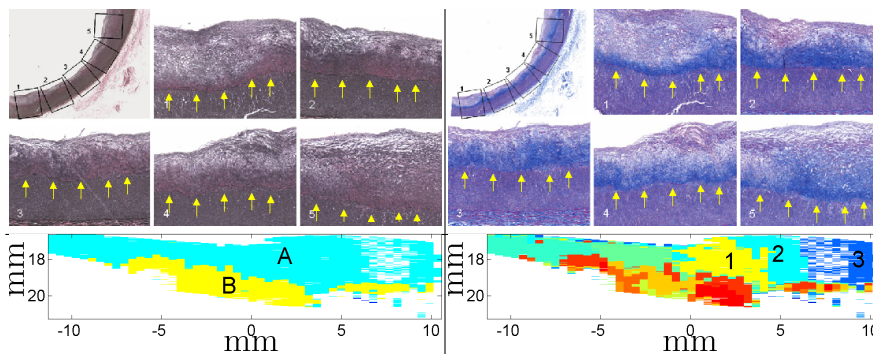


Fig. 5. (Top) Histological results for the region labeled (C) in Fig. 4 (c). (Top Left) Verhoeff van Gieson shows a gradual degradation of the internal elastic lamina from regions 1-5. (Top Right) Masson's trichrome shows a gradual increase in collagen from regions 1-5. (Bottom) Cluster membership corresponding to the yellow region in Fig. 4 (a). (Bottom Left) Three clusters: Two clusters differentiate between materials in the arterial wall (A, B). The third cluster (dark blue) contains noise. (Bottom Right) Eighteen clusters: Three components of the plaque are visible at the right side of the image (1-3).

4 Discussion

The response of a Kelvin material, such as arterial wall or atherosclerotic plaque, to an ARFI query is a peak displacement in the direction of the force followed by recovery at an exponential rate. Because the peak displacement and recovery rates are functions of material properties of the tissues themselves, ARFI induced displacement curves can be used to distinguish between tissue types. K-means clustering provides an automatic mechanism for classifying these ARFI response curves. The set of PCA coefficients for each of the displacements curves is a data representation that allows k-means to provide an effective clustering. Because PCA produces a low-dimensional approximation of the original data it allows the k-means algorithm to run faster, or equivalently it allows for more repetitions of the k-means algorithm in a fixed amount of time. We have shown preliminary results of using this technique to locate

an atherosclerotic plaque and to decompose it into three subregions of distinct elastin and collagen composition.

Our future work will include applying our method to other environments such as the deep venous system and other organ systems in in-vivo images. We expect to see relaxation curves as clean as those in Fig. 4 (b) during an in-vivo study. The image acquisition time for ARFI is orders of magnitude smaller than the cardiac cycle. Gallippi *et al.* [12] have successfully demonstrated physiological motion filters for cardiac gated in-vivo ARFI images.

We are interested in updating our methodology to overcome a limitation of the k-means algorithm. Our current method depends on *a priori* knowledge of the number of clusters to use. We are exploring two ways to provide a fully automatic segmentation of the ARFI image: by developing an optimization problem whose solution yields the number of salient clusters in the data and by developing prior distributions for the ARFI response curves of known tissue types. Our future work also will include extending our biomechanical model to include non-Kelvin materials.

References

1. Kavey, R.E.W., Daniels, S.R., Lauer, R.M., Atkins, D.L., Hayman, L.L., Taubert, K.: American Heart Association Guidelines for Primary Prevention of Atherosclerotic Cardiovascular Disease Beginning in Childhood. *Circulation* **107**(11) (2003) 1562–1566
2. Zhang, X., Kinnick, R.R., Fatemi, M., Greenleaf, J.F.: Noninvasive method for estimation of complex elastic modulus of arterial vessels. *Ultrasonics, Ferroelectrics and Frequency Control, IEEE Transactions on* **52** (2005) 642–652
3. Baldewings, R.A., Mastik, F., Schaar, J.A., Serruys, P.W., van der Steen, A.F.W.: Young's modulus reconstruction of vulnerable atherosclerotic plaque components using deformable curves. *Ultrasound in Medicine & Biology* **32** (2006) 201–210
4. Maurice, R.L., Daronat, M., Ohayon, J., Ékatherina Stoyanova, Foster, F.S., Cloutier, G.: Non-invasive high-frequency vascular ultrasound elastography. *Physics in Medicine and Biology* **50**(7) (2005) 1611–1628
5. Nightingale, K., Soo, M.S., Nightingale, R., Trahey, G.: Acoustic radiation force impulse imaging: in vivo demonstration of clinical feasibility. *Ultrasound in Medicine & Biology* **28** (2002) 227–235
6. Fung, Y.C.: *Biomechanics: Mechanical Properties of Living Tissues*. Springer (1993)
7. Palmeri, M.L., Sharma, A.C., Bouchard, R.R., Nightingale, R.W., Nightingale, K.R.: A finite-element method model of soft tissue response to impulsive acoustic radiation force. *Ultrasonics, Ferroelectrics and Frequency Control, IEEE Transactions on* **52** (2005) 1699–1712
8. Kiss, M.Z., Varghese, T., Hall, T.J.: Viscoelastic characterization of in vitro canine tissue. *Physics in Medicine and Biology* **49**(18) (2004) 4207–4218
9. MacQueen, J.B.: Some methods for classification and analysis of multivariate observations. In: *Proceedings of the Fifth Berkeley Symposium on Mathematical Statistics and Probability*. (1967)
10. Hasler-Rapacz, J., Nichols, T., Griggs, T., D.A., B., J., R.: Familial and diet-induced hypercholesterolemia in swine. lipid, apob, and apo-a-i concentrations and distributions in plasma and lipoprotein subfractions. *Arteriosclerosis, Thrombosis, and Vascular Biology* **14** (1994) 923–930
11. Dumont, D., Behler, R.H., Nichols, T.C., Merricks, E.P., Gallippi, C.M.: Arfi imaging for noninvasive material characterization of atherosclerosis. *Ultrasound in Medicine & Biology* (Special Issue dedicated to Frederic L. Lizzi) To appear.
12. Gallippi, C.M., Nightingale, K.R., Trahey, G.E.: Bss-based filtering of physiological and arfi-induced tissue and blood motion. *Ultrasound in Medicine & Biology* **29** (2003) 1583–1592